Numerical lifting line method for high speed free surface effect and/or ground effect

G.D. Thiart[1]

(Received August 1998; Final version January 1999)

A numerical lifting line method for the calculation of lift and induced drag on a straight wing of finite span in the proximity of a free surface, a ground surface, or a combination thereof is presented. The circulation distribution is expressed in terms of a Fourier sine series as for the classical Prandtl-Lanchester lifting line method. No approximations are introduced to linearize the lifting line equations, and the resulting nonlinear set of equations are solved iteratively. Results from the numerical lifting line method and approximate linearized methods available in the literature are compared for two practical wing planforms. Agreement between the two methods is shown to be good as long as the depth of submergence and/or ground clearance is large enough for the approximate method to be applicable.

Introduction

When a hydrofoil of finite span, i.e. a wing operating close to a free surface, is tested in a towing tank to obtain its hydrodynamic characteristics (lift, drag, and centre of pressure), the data have to be corrected for boundary effects, i.e. the influences of the tank bottom and side walls. Conversely, when a hydrofoil is used in shallow water or in a narrow canal, it is necessary to know what the effect of these restrictions is on the characteristics of the hydrofoil.

Approximations such as the lumped-vortex models used in aerodynamics[1] are usually employed to estimate the boundary effects, see for example Wadlin *et al.*[2] The applicability of these approximations is at best uncertain, especially for small depths of submergence or ground surface clearance. It is the purpose in this paper to present a numerical lifting line method which can be used to estimate the towing tank bottom/shallow water effect for high-speed hydrofoils, and to determine the range of applicability of the approximate formulations.

The classical Prandtl-Lanchester lifting line method for the calculation of lift and induced drag on a wing of finite span, as described by Bertin and Smith,[3] Anderson,[4] and Houghton and Carpenter,[5] amongst others, is only applicable for unbounded flows, and for wings with linear sectional lift characteristics. The iterative numerical lifting line method of Anderson *et al.*[6] extended the classical method to wings with nonlinear sectional lift characteristics. This numerical method was adapted by Thiart[7] to account for free-surface effects, by including a downwash correction. Here the latter method is modified to also model ground effect and the combination of free-surface and ground effect.

[1] Senior Lecturer, Department of Mechanical Engineering, University of Stellenbosch, Stellenbosch, 7600 South Africa

Mathematical model

General formulation

The lift and induced-drag coefficients for a wing of finite aspect ratio are computed, according to the lifting line method, from the circulation distribution $\Gamma(y)$, axialwash distribution $u_i(y)$ and downwash distribution $w_i(y)$ at the lifting line:

$$C_L = \frac{L}{\frac{1}{2}\rho U^2 S} = \frac{2A_R}{U^2 s^2}\int_{-s/2}^{s/2} [U + u_i(y)]\,\Gamma(y)\,dy \qquad (1)$$

$$C_{Di} = \frac{D_i}{\frac{1}{2}\rho U^2 S} = \frac{2A_R}{U^2 s^2}\int_{-s/2}^{s/2} w_i(y)\,\Gamma(y)\,dy \qquad (2)$$

The local circulation strength is expressed as follows in terms of the local chord length $c(y)$, effective onflow velocity $V_e(y)$, and sectional lift coefficient $C_l(y)$:

$$\Gamma(y) = \frac{1}{2} V_e(y)\; c(y)\; C_l(y) \qquad (3)$$

The magnitude of the effective onflow velocity is in turn expressed in terms of the free stream velocity and the velocities induced at the lifting line by the trailing vorticity associated with the lifting line and the proximity of boundaries:

$$V_e(y) = \sqrt{[U + u_i(y)]^2 + [w_i(y)]^2} \qquad (4)$$

The sectional lift coefficient is assumed to be a known function of the local effective angle of attack $\alpha_e(y)$ only, which is in turn a function of the geometrical angle of attack $\alpha(y)$, the zero-lift angle of attack $\alpha_0(y)$, and the induced angle of attack $\alpha_i(y)$:

$$\alpha_e(y) = \alpha(y) - \alpha_0(y) - \alpha_i(y) \qquad (5)$$

where

$$\alpha_i(y) = \arctan\left[\frac{w_i(y)}{U + u_i(y)}\right] \qquad (6)$$

Finally, the induced velocities are dependent on the circulation distribution, as will be detailed in the following subsections for the various cases of ground effect, free-surface effect, and the combination of ground and free-surface effect. These equations plus equations (1) to (6)

are solved iteratively, starting from an initial circulation distribution which, for the results presented here, is the circulation distribution obtained by means of the classical Prandtl-Lanchester lifting line method for a wing in unbounded flow and with linearized sectional lift characteristics. The circulation distribution, induced velocities, etc. are also obtained in the process, in terms of numerical values at the finite number of sections along the lifting line at which the chord length, the two-dimensional lift coefficient, and the geometrical and zero-lift angles of attack are defined.

Induced velocities for unbounded flow

For this case, the expressions for the induced velocities are the same as for the classical lifting line theory, i.e.

$$u_{i\infty}(y) = 0 \tag{7}$$

$$w_{i\infty}(y) = \frac{1}{4\pi}\int_{-s/2}^{s/2} \frac{d\Gamma}{dy}(\eta)\,\frac{1}{y-\eta}\,d\eta \tag{8}$$

Induced velocities for ground effect

Ground effect for a lifting line of strength $\Gamma(y)$ at height h above a ground surface is simulated[1] by placing an image lifting line of strength $-\Gamma(y)$ at a distance $2h$ below the lifting line, as illustrated in Figure 1. The additional induced velocities (to be added to those for the unbounded flow case) are given by

$$u_{iG}(y,h) = -\frac{h}{2\pi}\int_{-s/2}^{s/2} \Gamma(\eta)\,\frac{1}{\left[4h^2+(y-\eta)^2\right]^{\frac{3}{2}}}\,d\eta \tag{9}$$

$$w_{iG}(y,h) = -\frac{1}{4\pi}\int_{-s/2}^{s/2} \frac{d\Gamma}{dy}(\eta)\,\frac{y-\eta}{4h^2+(y-\eta)^2}\,d\eta \tag{10}$$

Induced velocities for high-speed free-surface effect

Free surface effect at large Froude numbers (i.e. high speed) for a lifting line of strength $\Gamma(y)$ at depth of submergence d below a free surface is simulated[1] by placing an image lifting line of strength $+\Gamma(y)$ at a distance $2d$ above the lifting line, as illustrated in Figure 2. The additional induced velocities (to be added to those for the unbounded flow case) are given by

$$u_{iF}(y,d) = u_{iG}(y,d) \tag{11}$$

$$w_{iF}(y,d) = -w_{iG}(y,d) \tag{12}$$

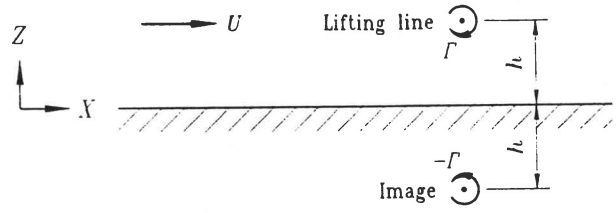

Figure 1 Section through lifting line and image for ground effect

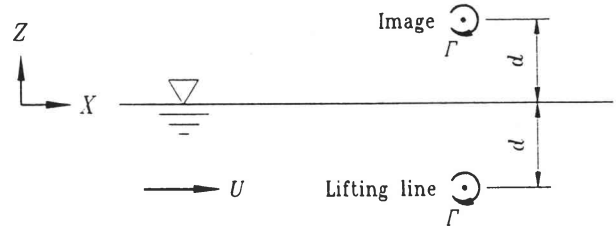

Figure 2 Section through lifting line and image for high-speed free-surface effect

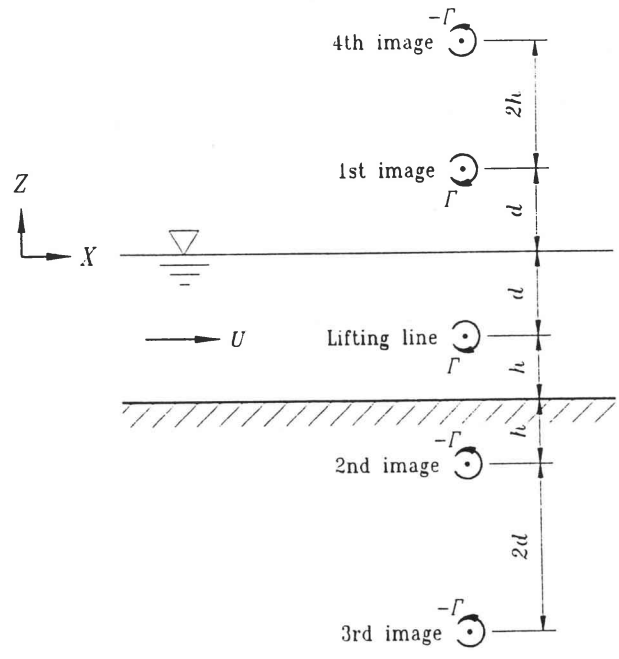

Figure 3 Section through lifting line and first 4 images for combined high-speed free-surface and ground effect

Induced velocities for combined high-speed free-surface and ground effect

Free surface effect at large Froude numbers combined with ground effect for a lifting line of strength $\Gamma(y)$ at depth of submergence d below a free surface and height h above a ground surface is simulated[2] by placing a series of image lifting lines of alternating strengths $\pm\Gamma(y)$ above and below the lifting line, as illustrated in Figure 3. The additional induced velocities (to be added to those for the unbounded flow case) are given by

$$u_{iFG}(y,d,h) = \frac{1}{2\pi}\int_{-s/2}^{s/2}\Gamma(\eta)\sum_{j=1}^{\infty}(-1)^k\frac{ld+mh}{\left[4(ld+mh)^2+(y-\eta)^2\right]^{\frac{3}{2}}}d\eta \tag{13}$$

$$w_{iFG}(y,d,h) = \frac{1}{4\pi}\int_{-s/2}^{s/2}\frac{d\Gamma}{dy}(\eta)\sum_{j=1}^{\infty}(-1)^m\frac{y-\eta}{4(ld+mh)^2+(y-\eta)^2}d\eta \tag{14}$$

where $k = \text{int}[(j+4)/4]$, $m = \text{int}[(j+2)/4]$, and $l = \text{int}[(j+1)/2] - m$.

Note that equations (9) to (10) can be recovered from equations (13) to (14) by taking only the terms for $j = 2$, and that equations (11) to (12) can be recovered from equations (13) to (14) by taking only the terms for $j = 1$.

Numerical model

Representation of the circulation distribution

In the numerical lifting line methods of Anderson *et al.*[6] and Thiart,[7] the circulation distribution is expressed in terms of piecewise linear or quadratic curve fits. Near the wing tips the magnitude of the circulation changes rapidly (to zero at the wing tips), with the result that the linear or quadratic representations are inaccurate there. Consequently it is necessary to divide the lifting line into a fairly large number of sections (100+) in order to obtain accurate results, as a result of which the methods are prone to divergence, and usually heavy underrelaxation is required to obtain a solution, if at all. For the method presented here, the circulation distribution is expressed in terms of a Fourier sine series, as for the classical Prandtl-Lancaster lifting line method:

$$\Gamma(\theta) = 2sU\sum_{n=1}^{\infty}A_n\sin n\theta \tag{15}$$

where θ is a transformation variable defined by $y = -(s/2)\cos\theta$. As will be shown later, much coarser subdivisions of the lifting line (≈30 sections) are sufficient to produce accurate solutions.

The numerical solution procedure is started with the classical linear solution which is the truncated Fourier series

$$\Gamma(\theta) = 2sU\sum_{n=1}^{N}A_n\sin n\theta \tag{16}$$

During the iteration process the circulation distribution is updated by means of equation (3), using the latest values of induced velocities at the sections along the lifting line. It is necessary to do an inverse Fourier transformation on the result to obtain the circulation distribution Fourier coefficients, and, due to the effect of aliasing,[8] it is only possible to calculate half as many Fourier coefficients as there are sections. Consequently, the actual representation of the nonlinear circulation distribution is given by

$$\Gamma(\theta) = 2sU\sum_{n=1}^{N/2}A_n\sin n\theta \tag{17}$$

where

$$A_n = \frac{1}{\pi sU}\int_0^{\pi}\Gamma(\theta)\sin n\theta\, d\theta \tag{18}$$

The integrals defined by equation (13) are evaluated numerically, using piecewise quadratic curve fits for Γ as function of θ.

Calculation of the induced velocities

The expressions for the induced velocities can be written in the following general form, covering all four cases under consideration:

$$u_i(\theta) = \int_0^{\pi}\Gamma(\phi)\,F_u(\phi,\theta)\sin\phi d\phi \tag{19}$$

$$w_i(\theta) = \frac{U}{\sin\theta}\sum_{n=1}^{N/2}nA_n\sin n\theta + \int_0^{\pi}\frac{d\Gamma}{d\theta}(\phi)\,F_w(\phi,\theta)\,d\phi \tag{20}$$

The first term in equation (20) represents $w_{i\infty}$, and is obtained analytically from equation (8). The remaining two terms in equations (19) and (20) represent the effect of the images, and the integrals contained in them are evaluated numerically using piecewise quadratic curve fits for Γ, F_u, $d\Gamma/d\theta$ and F_w as functions of the dummy variable ϕ. The functions F_u and F_w are defined implicitly by equations (9) and (10), equations (11) and (12), or equations (13) and (14), as appropriate. For the most general case, i.e. when $U_i = U_{i\infty} + U_{iFG}$ and $W_i = W_{i\infty} + W_{iFG}$, they are as follows:

$$F_u(\phi,\theta) = \frac{2s}{\pi}\sum_{j=1}^{\infty}(-1)^k\frac{ld+mh}{\left[16(ld+mh)^2+s^2(\cos\phi-\cos\theta)^2\right]^{\frac{3}{2}}} \tag{21}$$

$$F_w(\phi,\theta) = \frac{s}{2\pi}\sum_{j=1}^{\infty}(-1)^m \frac{\cos\phi-\cos\theta}{16(ld+mh)^2+s^2(\cos\phi-\cos\theta)^2} \quad (22)$$

In the case of combined free-surface and ground effect, these functions need only be evaluated for a finite number of images. It has been found by numerical experimentation that the number of images required for accurate computations can be taken as the nearest integer value to $100/\min[d/s, h/s]$.

Calculation of the lift and induced drag

The coefficients of lift and induced drag are obtained by integration of equations (1) and (2), analytically in part by using the expression for the circulation distribution given by equation (17) and the first term in the expression for the downwash given by equation (20). The results for the most general case are as follows:

$$C_L = \pi A_R A_1 + \frac{A_R}{U^2 s}\int_0^{\pi} u_{iFG}(\theta)\,\Gamma(\theta)\sin\theta\,d\theta \quad (23)$$

$$C_{Di} = \pi A_R \sum_{n=1}^{N/2}(A_n)^2 + \frac{A_R}{U^2 s}\int_0^{\pi} w_{iFG}(\theta)\,\Gamma(\theta)\sin\theta\,d\theta \quad (24)$$

The remaining integrals in equations (23) and (24) are evaluated numerically using piecewise quadratic curve fits for Γ, u_i and w_{iFG} as functions of θ.

Results

The numerical model described in the previous section was programmed in double precision FORTRAN77. The program was then used to compute the lift and induced-drag coefficients for a wing with circular arc cross-sections with maximum camber equal to 4.375% of chord length. For such cross-sections the zero-lift angle (α_0) and two-dimensional lift curve slope (C_l') predicted by thin airfoil theory are equal to $-5°$ and 2π, respectively. These two values were used for all the results presented in the two subsections that follow.

In order to ensure convergence, it was necessary to underrelax the downwash; an underrelaxation factor equal to $0.5^{0.2N}$ was used throughout. The lifting line was subdivided by means of the semi-circle method, giving an equi-$\Delta\theta$ spacing. Convergence was assumed to be reached when the product of the absolute changes in lift and induced-drag coefficients was less than 10^{-16} for ten consecutive iterations.

Convergence

The lift curve slope and induced drag for a wing of finite aspect ratio can be expressed as follows:[4]

$$C_L' = \frac{C_l'}{1+C_l'(1+\tau)/\pi A_R} \quad (25)$$

$$C_{Di} = \frac{C_L^2}{\pi A_R}(1+\delta) \quad (26)$$

Here τ is a lift efficiency factor and δ an induced-drag factor which, according to linear lifting line theory, are both equal to zero for a wing with an elliptical planform.

Computations were carried out to determine values for τ and δ as function of $\Delta\theta$ for four different $A_R = 5$ wings: the first with an elliptical planform, the second with a rectangular planform, the third with a triangular planform, and the fourth with a tapered planform with a tip-to-root chord ratio of 0.3. These computations were carried out for two angles of attack: 0° and 5°, and some of the results are presented in Figures 4 to 6.

Figure 4 shows that the values of τ for all four planforms and for both angles of attack becomes grid-independent at $\Delta\theta \approx 3°$, i.e. for $N \approx 60$. The same applies for the values of δ, Figure 5 (the results for $\alpha = 5°$ are not shown, as they are almost identical with the $\alpha = 0°$ results). The number of iterations required to reach convergence for the rectangular wing is less than 200 for $\alpha = 0°$ and less than 300 for $\alpha = 5°$ at $\Delta\theta = 3°$, as shown in Figure 6. The number of iterations required to reach convergence for the other three planforms are almost identical to those for the rectangular wing, and are therefore not shown.

Boundary effects

The proposed numerical method was further validated by comparing computed results with those of the analytical approximations presented by Von Kármán and Burgers.[1] These approximations were derived by means of lumped-vortex systems, i.e. the wing and each one of its images are represented by a single horseshoe vortex, the trailing 'legs' of which are separated by a distance βs.

The factor β can be determined[5] by the two requirements that (i) the single horseshoe vortex must have the same strength as the sum of the trailing vortices in the lifting line representation of the wing, and (ii) that the lift must be the same for both methods. The result can be expressed in terms of the Fourier coefficients of the circulation distribution computed by means of the conventional linear line method:

$$\beta = \frac{\pi A_1}{4(A_1 - A_3 + A_5 - A_7 + \ldots)} \quad (27)$$

According to the approximations, the changes in lift and induced drag can be written as follows:

$$\frac{\Delta C_L}{C_L} = \frac{1}{\pi A_R}\left[-\sigma C_L' + \frac{2\pi A_R + C_l'}{\pi A_R + C_l'}\epsilon C_L\right] \quad (28)$$

and

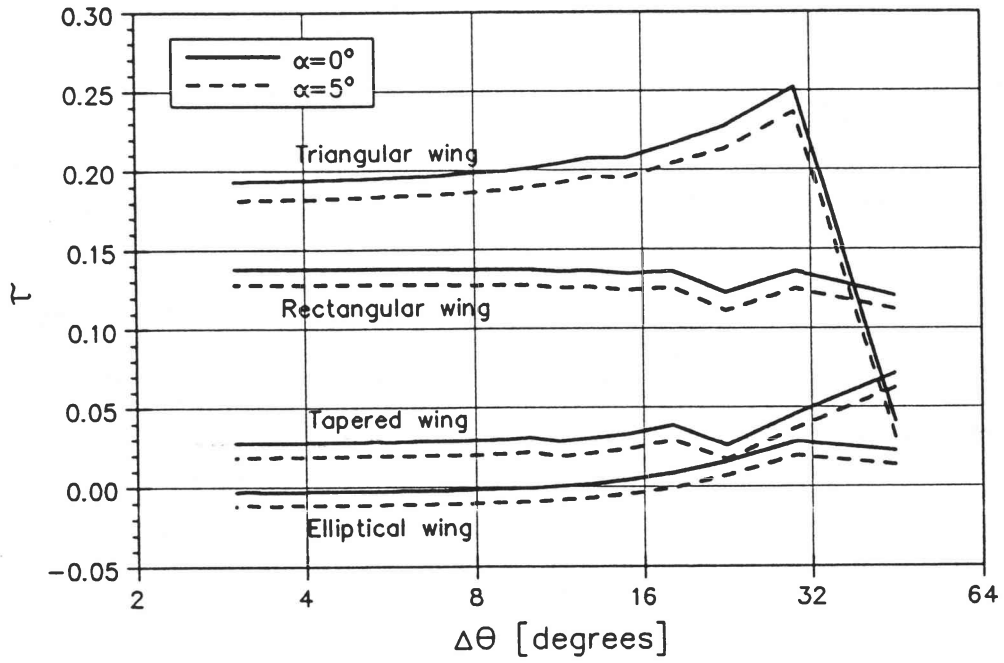

Figure 4 Convergence of lift efficiency factor for four wing planforms and two angles of attack

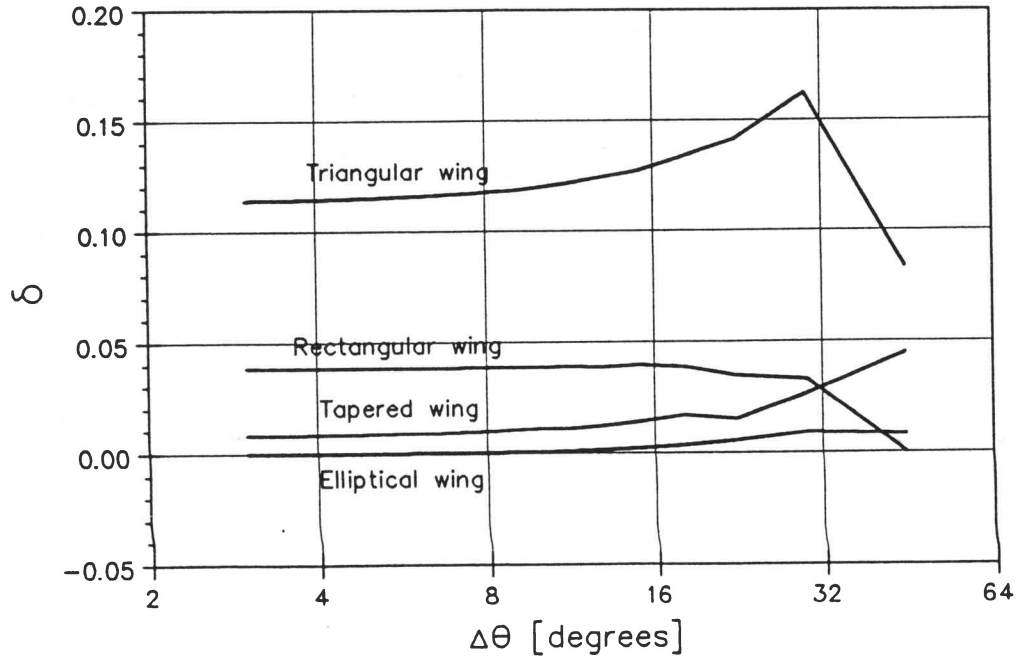

Figure 5 Convergence of induced-drag factor for four wing planforms at $\alpha = 0°$

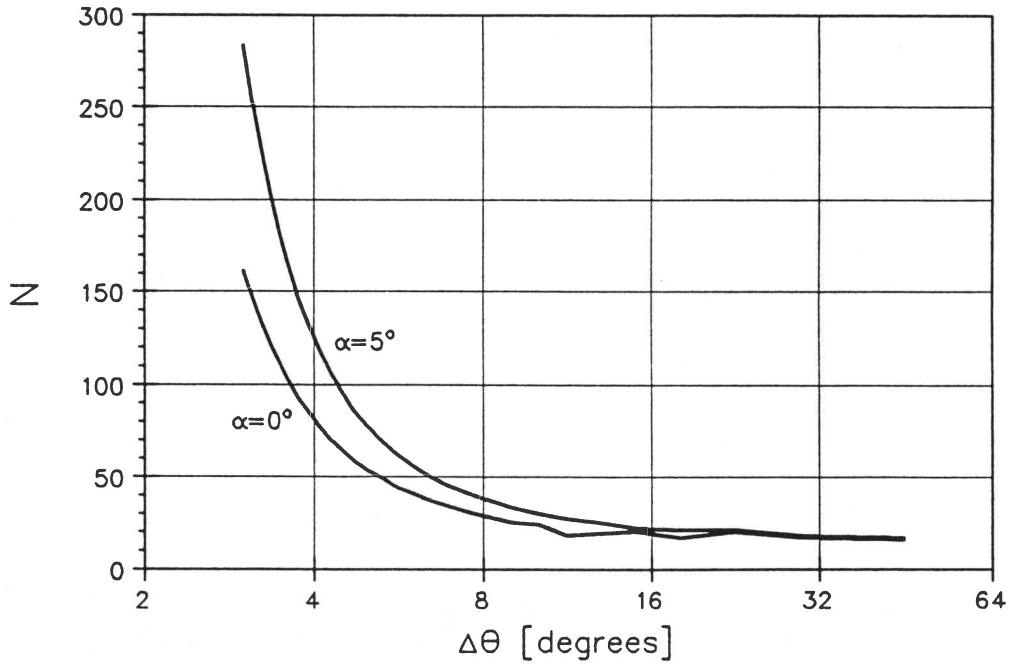

Figure 6 Number of iterations required for convergence (rectangular wing)

$$\frac{\Delta C_{Di}}{C_L^2} = \frac{1}{\pi A_R}\left[\sigma\left(1 - \frac{2}{\pi A_R} C_L'\right) + \frac{2}{\pi A_R + C_l'}\epsilon C_L\right] \tag{29}$$

The factors σ and ϵ are the values of the average downwash and axialwash, respectively, nondimensionalised with respect to U, induced at the lifting line by the image or images of the horseshoe vortex or vortices representing the wing. Expressions for these factors are as follows for ground effect,

$$\sigma_G = -\frac{1}{8\beta^2}\ln\left[1 + \left(\frac{\beta s}{2h}\right)^2\right] \tag{30}$$

$$\epsilon_G = -\frac{1}{4\beta^2}\left[\sqrt{1 + \left(\frac{\beta s}{2h}\right)^2} - 1\right] \tag{31}$$

and as follows for high-speed free-surface effect:

$$\sigma_F = +\frac{1}{8\beta^2}\ln\left[1 + \left(\frac{\beta s}{2d}\right)^2\right] \tag{32}$$

$$\epsilon_F = -\frac{1}{4\beta^2}\left[\sqrt{1 + \left(\frac{\beta s}{2d}\right)^2} - 1\right] \tag{33}$$

For combined free-surface and ground effect, the factors can be obtained by summing the influences of all the images, the summations being similar to those of equations (13) and (14):

$$\sigma_{FG} = \frac{1}{8\beta^2}\sum_{j=1}^{\infty}(-1)^m \ln\left[1 + \left(\frac{\beta s}{2\,(ld + mh)}\right)^2\right] \tag{34}$$

$$\epsilon_{FG} = \frac{1}{4\beta^2}\sum_{j=1}^{\infty}(-1)^k \left[\sqrt{1 + \left(\frac{\beta s}{2\,(ld + mh)}\right)^2} - 1\right] \tag{35}$$

Numerical results computed by means of the proposed nonlinear lifting line method for ground effect and for high-speed free-surface effect are compared with the corresponding analytical approximations in Figures 7–10 for two practical $A_R = 5$ wings: one with a rectangular planform and the other one with a tapered planform with a tip-to-root chord ratio of 0.3. For these same two wings numerical results computed by means of the proposed nonlinear lifting line method for combined ground effect and high-speed free-surface effect are compared with the corresponding analytical approximations in Figures 11–12. These latter results were computed for combinations of h/s and d/s such that $h/s + d/s = 1$. All the results were computed for angle of attack $\alpha = 0°$.

The ground-effect approximation for variation in lift of the rectangular wing corresponds to within one percentage point with the numerical result down to a ground clearance of $h/s \approx 0.1$ (≈ 0.5 chord lengths), and for the tapered wing down to a ground clearance of $h/s \approx 0.2$ (≈ 1 mean chord length), Figure 7. The differences for variation in induced drag are everywhere less than one percentage point, Figure 8.

The high-speed free-surface effect approximation for variation in lift of the rectangular wing corresponds to within one percentage point with the numerical result down to a submergence of $d/s \approx 0.2$ ($\approx$1 chord length), and for the tapered wing down to a submergence of $d/s \approx 0.3$ (≈ 1.5 mean chord lengths), Figure 9. The differences for variation in induced drag is less than one percentage

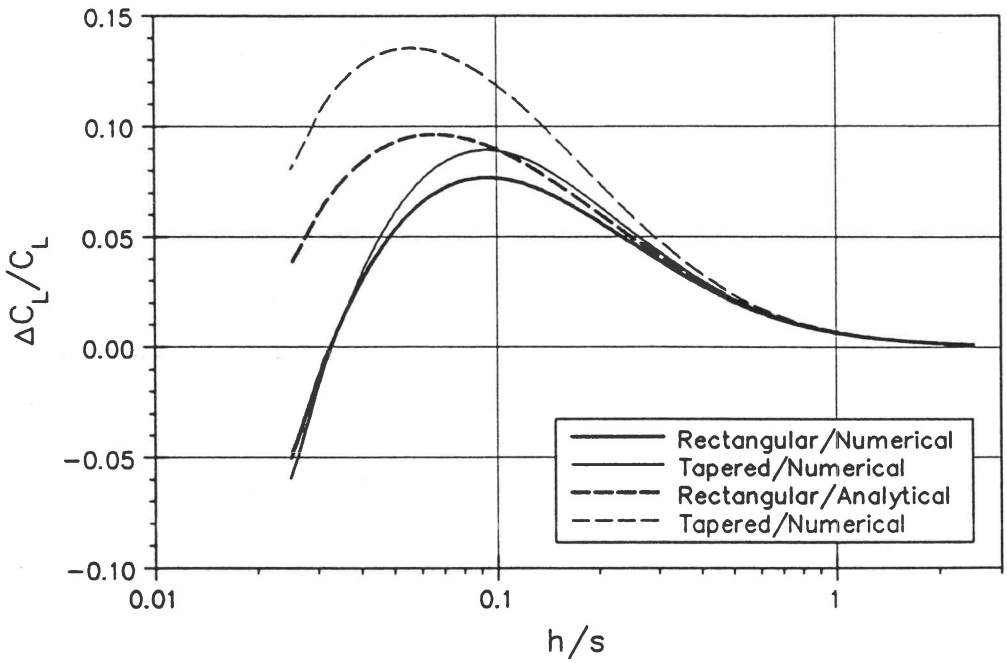

Figure 7 Variation in lift as function of ground clearance

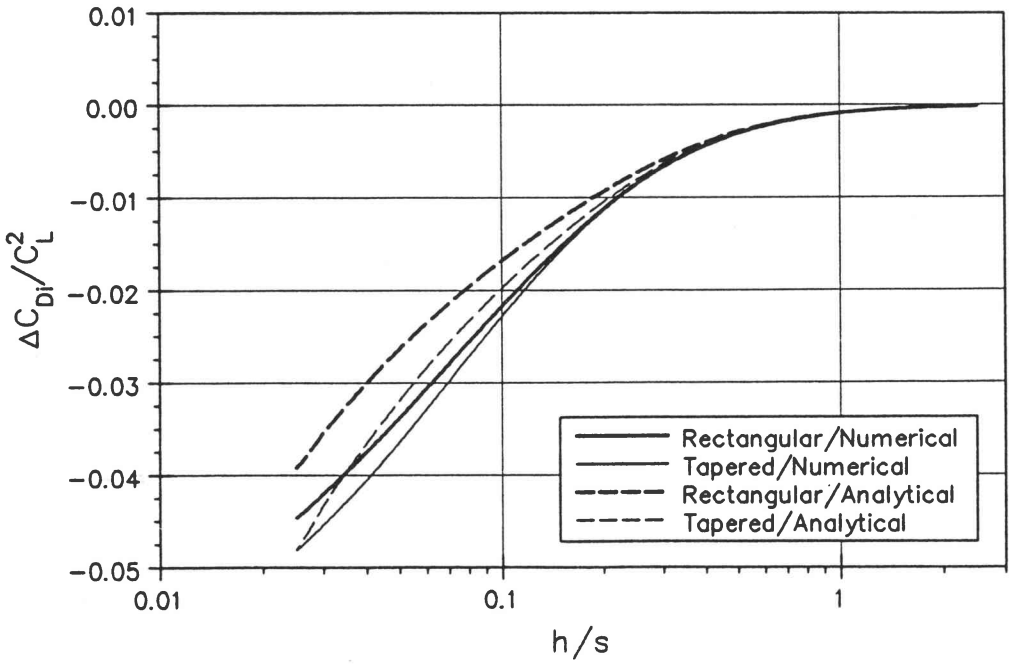

Figure 8 Variation in induced drag as function of ground clearance

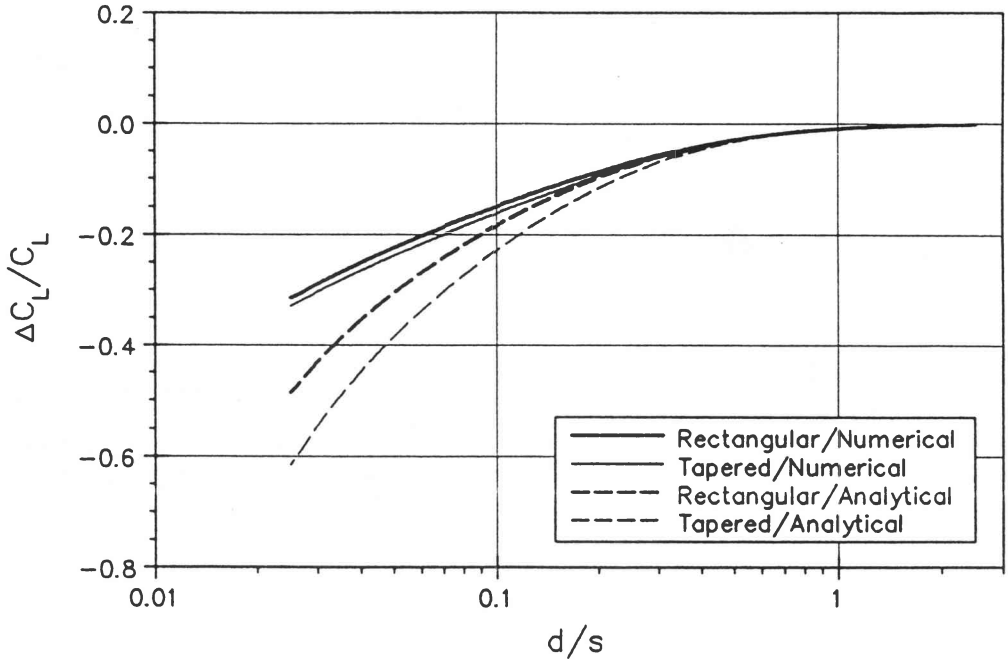

Figure 9 Variation in lift as function of submergence depth

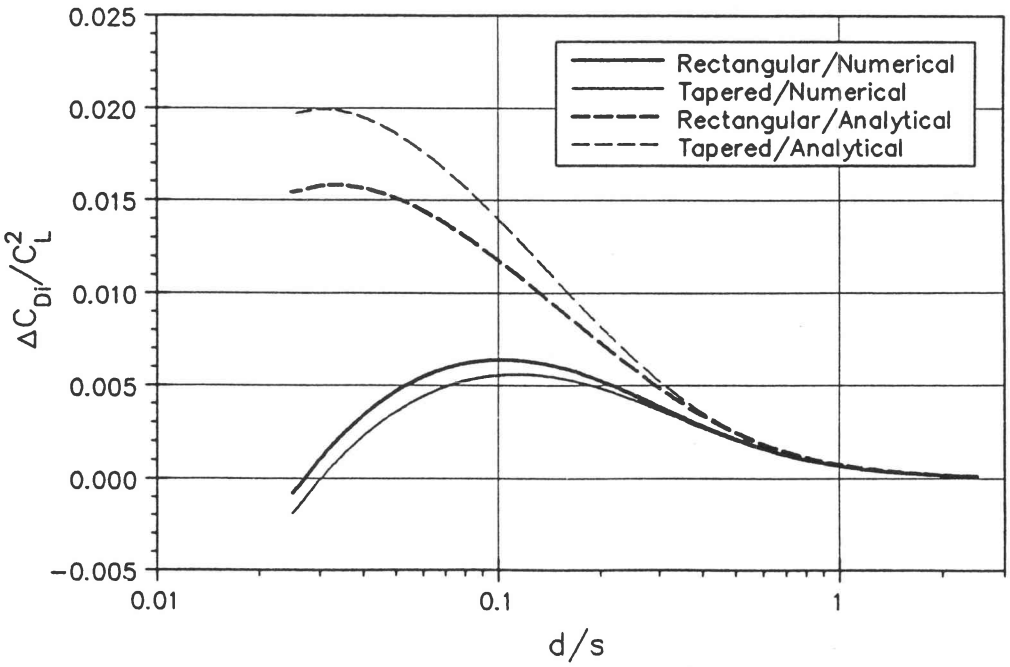

Figure 10 Variation in induced drag as function of submergence depth

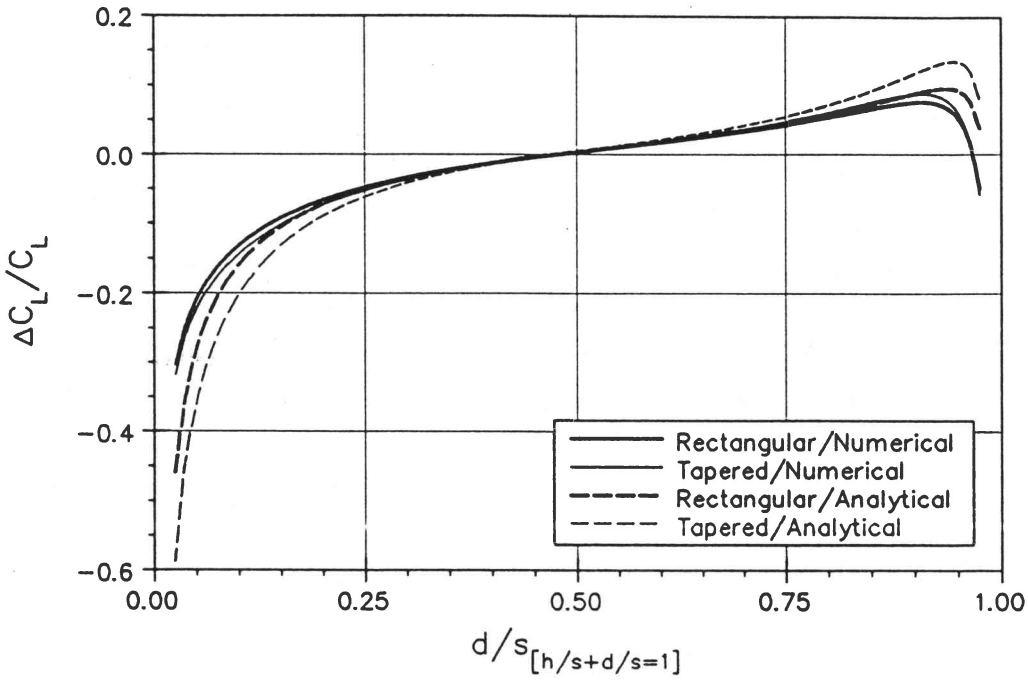

Figure 11 Variation in lift as function of submergence depth and bottom clearance

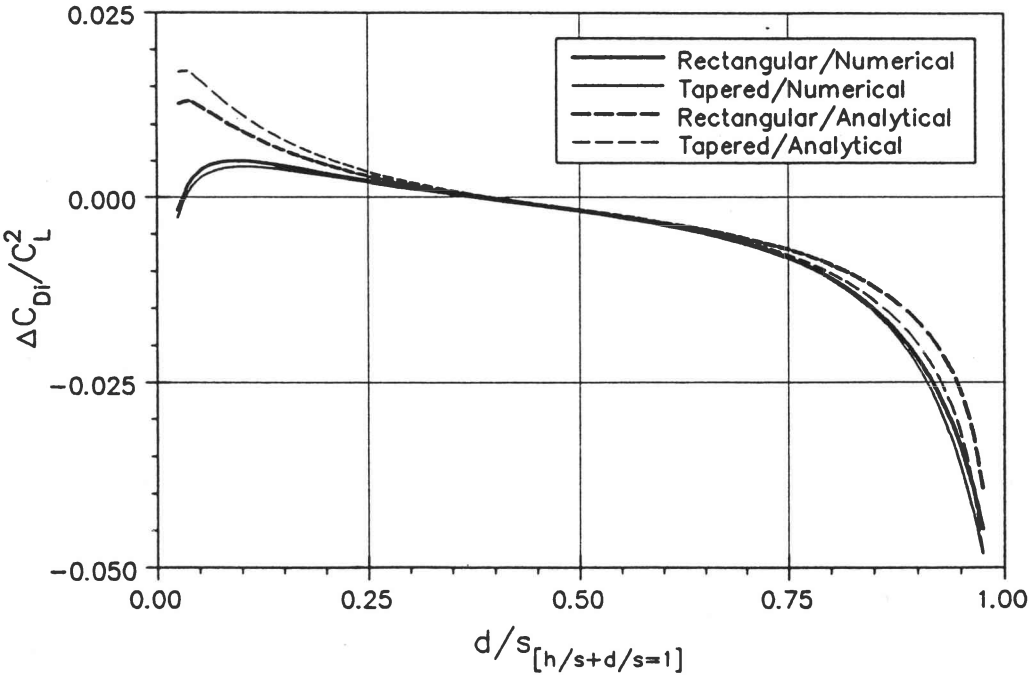

Figure 12 Variation in induced drag as function of submergence depth and bottom clearance

point down to a submergence of $d/s \approx 0.06$ (≈ 0.3 chord lengths) for the rectangular wing, and down to a submergence of $d/s \approx 0.1$ (≈ 0.5 mean chord lengths) for the tapered wing, Figure 10.

The combined ground effect and high-speed free-surface effect approximation for variation in lift of the rectangular wing corresponds to within one percentage point with the numerical result between $d/s \approx 0.15$ and $h/s \approx 0.15$ (both ≈ 0.75 chord lengths), and for the tapered wing between $d/s \approx 0.25$ and $h/s \approx 0.2$ ($\approx$1.25 and 1 mean chord length, respectively), Figure 11. The differences for variation in induced drag is less than one percentage point for $d/s \succ\approx 0.05$ (≈ 0.25 chord lengths) for the rectangular wing, and for $d/s \succ\approx 0.08$ (≈ 0.4 mean chord lengths) for the tapered wing, Figure 12.

Conclusion

A numerical lifting line method for the computation of lift and induced drag of a wing in the proximity of a ground and/or a free surface has been presented. It has been shown that the method is both robust and accurate. Computations have been presented to show that the method can be used to estimate the range of accuracy of classical analytical approximations for computation of lift and induced drag.

The method can be used to compute towing tank corrections to measured data, if the clearance between the wing tips and towing tank side walls are large. Work is currently in progress to extend the method to also take into account the effect of side walls.

References

1. Von Kármán T & Burgers JM. General aerodynamic theory – perfect fluids. *Aerodynamic Theory,* **II**, Dover, New York, 1963.

2. Wadlin KL, Shuford CL & McGehee JR. A theoretical and experimental investigation of the lift and drag characteristics of hydrofoils at subcritical and supercritical speeds. *Langley Aeronautical Laboratory Report 1232.* US Government, 1956.

3. Bertin JJ & Smith ML. *Aerodynamics for Engineers.* Prentice-Hall, Englewood Cliffs, 1979.

4. Anderson JD. *Fundamentals of Aerodynamics.* 2nd edn. McGraw-Hill, New York, 1991.

5. Houghton EL & Carpenter PW. *Aerodynamics for Engineering Students.* 4th edn. Edward Arnold, London, 1993.

6. Anderson JD, Corda S & Van Wie DM. Numerical lifting line theory applied to drooped leading-edge wings below and above stall. *J. Aircr.*, 1980, **17**, pp.898–904.

7. Thiart GD. Numerical lifting line theory for a hydrofoil near a free surface. *R&D Journal*, 1994, **10**, pp.18-23.

8. Newland DE. *Random Vibrations and Spectral Analysis.* Longman, London, 1975.